Combustion instability during starting of a turbocharged diesel engine including biofuel effects

Evangelos G. Giakoumis[1], Athanasios M. Dimaratos[2], Constantine D. Rakopoulos[3], Dimitrios C. Rakopoulos[4]

Abstract: A series of starting tests was conducted on a turbocharged diesel engine investigating combustion instability for various coolant temperatures, ranging from 20 to 80oC, and fuel blends (neat diesel, blend of diesel with 30% biodiesel and blend of diesel with 25% *n*-butanol). A statistical analysis was performed in order to quantify the effects of the coolant temperature and fuel properties on the extent of the instability phenomena. As expected, the engine thermal status was found to play an influencing role, with cold starting leading to combustion instability; difference up to 38 bar between successive cycles was documented. The biodiesel blend exhibited higher instability and the *n*-butanol one higher absolute pressures but somewhat more stable operation. Both biofuel blends led to higher in-cylinder pressure irregularities compared to the neat diesel operation. For all examined blends, instability phenomena were still apparent even after several seconds from the engine start-up.

Keywords: Diesel engine; Starting; Combustion instability; Biodiesel; N-butanol

---

[1]Associate Professor, School of Mechanical Engineering, National Technical University of Athens, 15780 Athens, Greece (corresponding author). E-mail: vgiakms@central.ntua.gr

[2] Research Associate, Laboratory of Applied Thermodynamics, Dept. of Mechanical Engineering, Aristotle University of Thessaloniki, 54124, Thessaloniki, Greece, E-mail: dimarathan@gmail.com

[3] Professor Emeritus, School of Mechanical Engineering, National Technical University of Athens, 15780 Athens, Greece. E-mail: cdrakops@central.ntua.gr

[4]Research Associate, School of Mechanical Engineering, National Technical University of Athens, 15780 Athens, Greece. E-mail: dimracop@central.ntua.gr

Introduction

Nowadays, manufacturers of vehicular internal combustion engines are required to address on the one hand the strict emission regulations and on the other the customer demand for low-consumption vehicles with good driveability. In order to successfully meet these objectives, the diesel engine has emerged as a very promising alternative to gasoline engines, based on superior fuel economy, robust operation, higher torque, and ease of turbocharging.

There are specific areas of a turbocharged diesel engine operation, however, that remain problematic, most notably the transient behavior (from low loads), which is realized in the form of poor acceleration and overshoot in exhaust emissions (Rakopoulos and Giakoumis, 2009; Watson and Janota, 1982). Another major area, where the diesel engine suffers compared to gasoline engines, is starting, owing to this operation characteristically being influenced by combustion instability phenomena, particularly at low ambient temperatures (Henein et al., 1992).

With reference to the coolant and ambient temperature, starting is classified as cold or hot. Owing to significantly worse unstable operation, it is not surprising that cold starting has, in general, been researched much more compared to hot starting. Typical phenomena experienced by the engine during cold starting are an increased amount of engine-out soot, HC and CO emissions. The fact that the exhaust after-treatment devices have not yet reached their operating temperature leads to a considerable amount of vehicle-out emissions too. For example, it has been reported that a diesel engine may emit up to seven times more particulate matter during cold operation than under warm conditions (Bielaczyz et al., 2001), whereas more than 70% of the diesel particulates are produced during the first minutes of the NEDC (New European Driving Cycle), where the engine operates under not fully warmed-up conditions (Mathis et al., 2005). In order to take these serious environmental issues into account, the legislation in the European Union required from the year 2000 that the new vehicles are tested during the type approval process with the engine cold started (Rakopoulos and Giakoumis, 2009). The same cold starting procedure is nowadays almost universally applicable to European, US and worldwide driving and engine cycles.

When a vehicular engine is started, the following phases can be identified. Initially, (cranking phase), the engine accelerates rapidly with the assistance of the electric starter; the latter being an integral part of an automobile's starting system. The next, much slower, acceleration phase is then accomplished without the need for external assistance, until, finally, the point where stabilization to the idling speed is achieved. Unfortunately, during a diesel engine's cold starting event, the auto-ignition process may prove unreliable, particularly at temperatures below 0°C. This is due to an inherent feature of the diesel engine's operation, namely auto-ignition, which often proves unsuccessful during starting, resulting in engine/cylinder misfire.

When the engine misfires, the power derived from combustion is not adequate to overcome the increased heat losses to the cold cylinder walls. Further, at low ambient temperatures, the high lubricant viscosity and the still 'wide' piston ring-cylinder wall clearances unarguably lead to a considerable increase of friction losses too. As a result of the above, it is not always feasible for a combustible air-fuel mixture to be formed. This, in turn, results in certain combustion irregularities known as *combustion instability.* It should be emphasized that at very low ambient temperatures, even complete starting failure may be encountered (Henein et al., 1992; Kobayashi et al., 1984).

Previous research, mainly on naturally aspirated engines (Henein et al., 1992; Kobayashi et al., 1984; Phatak and Nakamura, 1983), has identified many influential parameters that are responsible for the occurrence of combustion instability. The temperature of the environment is perhaps the most obvious parameter, with the possibility of misfire increasing the lower the ambient temperature. A low fuel cetane number further enhances the instability phenomena owing to its interrelation with ignition delay, as does the compression ratio. The lower the cranking speed, the more time is available for heat and blow-by losses. Fuel injection timing and pattern play a critical role too, with advanced injection enhancing instability. Lastly, the amount of residual gas as well as the various starting aids such as glow plugs, etc. are influential parameters too.

The target of the present study is to expand on the experimental investigation of diesel starting with the focus on combustion instability phenomena, quantify these effects through a relevant statistical analysis, and subsequently shed more light into the underlying mechanisms. To this aim, an extended set of experimental tests was conducted on a medium-duty, turbocharged diesel engine. An important aspect of the current investigation is that it focuses on all possible starting cases that may be

experienced during daily vehicle driving, i.e., cold, warm and hot, providing also useful comparisons between them.

In parallel, an increasing effort to develop alternative fuel sources has been in progress during the last decades, sparked by two main facts: diminishing oil reserves, as well as the need to more efficiently control exhaust emissions and CO_2. Among these alternate fuels, biofuels have assumed a key role (Graboski and McCormick, 1998). Vegetable oils, their methyl-esters (biodiesels), dimethylether and various bioalcohols are the most vigorously investigated biofuels today. It is especially biodiesel that is considered the most promising alternative to diesel oil for CI engines. Main contributing factors are the close similarity of its properties to those of conventional diesel fuel, the fact that it can be blended with diesel at any proportion, whereas no changes are required in the existing distribution infrastructure (Graboski and McCormick, 1998; Giakoumis et al., 2012).

On the other hand, two traditional SI engine biofuels, namely ethanol and *n*-butanol (collectively referred to as bioalcohols), seem to be quiet promising for CI engines too. The rationale is located in their substantial potential for both CO_2 and PM emissions reduction (Hansen et al., 2005; Jin et al., 2011). Since the oxygen content in the alcohol molecule is higher compared to biodiesel, it is not surprising that the potential of alcohols for PM reduction is much higher compared to that of biodiesel. A further contributing factor here is the low cetane number of the alcohols, which results in a higher proportion of the combustion process being shifted into the premixed phase (Giakoumis et al., 2013).

Despite the extended research on the use of biofuels in diesel engines, the focus so far has almost exclusively, been on the regulated exhaust pollutants during steady-state (Graboski and McCormick, 1998; Hansen et al., 2005; Jin et al., 2011; Lapuerta et al., 2008; Rakopoulos et al., 2010) or, more recently, transient operation (Giakoumis et al., 2012; 2013). There is only a handful of works investigating the engine behavior during starting with biodiesel or alcohol-diesel fuel blends (e.g. Randazzo and Sodre, 2011; Rakopoulos et al., 2011a; Armas et al., 2013, 2015; Broatch et al., 2014; Cardenas et al., 2015); the emission of exhaust pollutants has been in the epicenter of these works too, with startability effects also considered.

It is strongly believed that with the continuously growing research on the use of alternative fuels in engines, their starting behavior should be thoroughly examined too to

give feedback on possible issues and limitations. Therefore, a second target of the current investigation is to extend the research on combustion instability phenomena during starting, when biofuel blends are applied. Owing to specific restrictions of the experimental installation, however, these tests have been limited to the hot starting cases only. The examined blends were:

- a blend of 70% diesel with 30% biodiesel, and
- a blend of 75% diesel with 25% n-butanol.

Through the analysis that will be presented in the next paragraphs, it is believed that useful overall conclusions on the diesel engine starting behavior will be deducted that can prove useful to the engine community.

A Brief Reminder on Basic Attributes of Biodiesel and *N*-Butanol

Biodiesel is produced by transesterification of vegetable oils, animal fats or recycled cooking oils. It consists of long-chain alkyl esters, containing two oxygen atoms per molecule (Graboski and McCormick, 1998; Giakoumis et al., 2012). The more widely used biodiesels today are rapeseed methyl-ester (RME) in Europe and soybean methyl-ester (SME) in the US. Biodiesel originating from palm, sunflower, cottonseed, waste cooking and tallow are often researched methyl esters in other regions of the world.

The major biodiesel advantage relative to diesel fuel is its renewability (Lapuerta et al., 2008). This is an extremely promising fact although other (conflicting) issues, such as food prices and biodiversity have gained increased attention recently. Emission of particulate matter, CO and HC are typically lower when biodiesel blends are applied, with a moderate increase in the respective NO_x emissions usually experienced (Giakoumis, 2012).

The major technical barriers associated with the use of biodiesel, on the other hand, are its production cost, its susceptibility to oxidation as well as its poor low-temperature properties. It is particularly the latter that play a significant (negative) role during the engine cold starting process, rendering it more difficult the higher the biodiesel percentage in the fuel blend (Giakoumis, 2013).

Butanol is a biomass-based renewable fuel too; it can be produced by alcoholic fermentation of sugar from various vegetable materials, agricultural residues, or even

from biomass such as wood or grasses. The more widely utilized alcohol today is alcohol, primarily owing to its low cost of production compare to butanol. Butanol, however, possesses ‘better’ properties than alcohol at least as regards its use in diesel engines, namely higher heating value and cetane number, lower vapor pressure, higher viscosity, less hydrophilic tendency, and (almost) perfect miscibility with diesel oil (Jin et al., 2011).

The relevant literature on butanol effects on diesel engine performance and emissions is increasing at high rates during the last years. The isomer that has most been experimented with and is also used in the present study is 1-butanol, widely referred to as *n*-butanol (normal butanol). It has a straight chain structure with the hydroxyl group at the terminal carbon ($CH_3CH_2CH_2CH_2OH$) (Yao et al., 2010).

The present research group has already significant experience on the performance and emissions of diesel engines when fuelled with blends of diesel fuel with *n*-butanol or biodiesel, having investigated the relevant phenomena under both steady-state (e.g. Rakopoulos et al., 2010; Rakopoulos, 2015) and transient (acceleration) conditions (e.g. Giakoumis et al., 2012, 2013; Rakopoulos et al., 2011b).

Experimental Set-up and Procedure

For the current experimental investigation, a Mercedes-Benz OM 366 LA, turbocharged DI bus diesel engine is employed, coupled to a hydraulic dynamometer; the basic technical data of the engine are provided in Table 1. Two notable features of the engine that influence its combustion (and emission) behavior are its retarded fuel injection timing in order to achieve low NO_x emissions, and the fuel-limiter (cut-off) function in order to avoid overshoot of exhaust smoke during demanding conditions such as transients.

The engine and turbocharger operating parameters measured and recorded continuously, as demonstrated schematically in Figure 1, are:

- engine speed (a Kistler shaft encoder was utilized, with the signal also used for time/crank angle reference);

- cylinder pressure (applying a Kistler miniature piezoelectric transducer, type 6051A, mounted on the cylinder head coupled to a Kistler charge amplifier, type 5007;
- Fuel pump rack position (measured through a Linear Variable Differential Transducer (LVDT), type DC25, manufactured by Solartron Metrology and connected mechanically to the fuel pump rack;
- Boost pressure (measured at two different locations, one immediately downstream of the turbocharger compressor, using a conventional manometer, and the second at the inlet manifold of the engine after the after-cooler. For the continuous measurement of boost pressure at the second location, a pressure transmitter manufactured by Wika, type A-10, is used.
- Turbocharger speed (a Garrett Turbo Speed Sensor was employed, the sensor placed on the compressor housing, in such a way that the sensor 'sees' both full and splitter blades. The output signal is a square-wave one at 1/8th the input frequency. The latter is simply one pulse per blade, as the blades pass in front of the sensor. Taking into consideration the number of compressor wheel blades, the turbocharger speed can then be calculated. The output signal is recorded continuously, whereas a conventional analogue tachometer (speed gauge) is also employed for an initial estimation of the turbocharger rotational speed.
- Exhaust pressures and temperatures at various locations were also measured during steady-state conditions with conventional analogue devices. Additionally, fuel consumption measurement was taken during steady-state operation with the use of a gravimetric fuel tank.

Table 2 summarizes the main information of the starting tests conducted at different coolant/oil temperatures. For each test, the pedal was fixed to a specific position corresponding to the desired engine idling speed and then the starter button was initiated. Overall, six tests were executed; four with the engine run on neat diesel oil with gradually increasing coolant/oil temperature, whereas two hot starting tests were conducted applying biofuel blends. Owing to some minor irregularities during the experimental procedure, the demanded engine speeds during the starting events are not uniform, as is evident in Table 2.

The biofuel blends tested under hot starting conditions were:

- a blend of 70% automotive low-sulfur diesel with 30% biodiesel (the latter originating from 50%-50% v/v sunflower and cottonseed oils), and
- a blend consisting of 75% diesel and 25% *n*-butanol v/v.

Table 3 provides the main physical and chemical properties of the diesel fuel and the biofuels used in the investigation.

Results and Discussion

Cold starting test No. 1

The first case of starting (test No. 1 in Table 2) was performed under cold conditions, with the coolant and lubricating oil temperatures being 20°C, i.e. at the lower limit foreseen by the current European legislation as regards the NEDC testing of new vehicles). The development of various engine and turbocharger operating parameters for this test, with the emphasis on the maximum cylinder pressure and the development of the engine speed/acceleration, is illustrated in Figure 2; the discussion that follows provides the opportunity to describe a typical starting event for an engine equipped with a mechanical-type fuel pump/governor.

Before the engine was started, the fuel pump rack was located at its minimum position (upper-right sub-diagram of Fig. 2). As soon as the engine was started, the governor forced the fuel pump rack to its maximum fueling position. During the first three cycles after the engine start-up, the initial sharp increase of the engine speed was supported by the assistance of the electric starter. After 1.4 s (three cycles), the starter was disengaged, and the engine accelerated by itself at a much slower rate. Throughout this period, there was an obvious lack of air supply to the cylinders owing to the still very low engine and turbocharger rotational speeds. As a result, locally high fuel-air ratios were experienced, that led to flame quenching (owing to oxygen shortage) and combustion deterioration. As the engine speed gradually increased, the rack moved progressively to lower fuel supply, until it ultimately assumed its final steady-state value after the engine had reached its idling, self-sustained speed (after approximately 40 engine cycles).

Even after the engine speed had stabilized, the thermal status of the engine kept changing as a much longer duration is generally required for the stabilization of the exhaust gas, coolant, lubricating oil, and cylinder and exhaust manifold wall temperatures. The apparent reason here is the latters' high thermal inertia. This thermal transition lasted for at least a few minutes, which is a relatively long period compared to the duration of the actual starting event, and affected the turbocharger response too.

The upper-left sub-diagram of Fig. 2 demonstrates explicitly the occurrence of combustion irregularity during the starting event, in the form of the rather highly unstable maximum cylinder pressure traces, particularly for the first 15 cycles (stage 1). For a more thorough understanding, a detailed view of the respective pressure diagrams during the engine cycles of stage 1 is provided in Figs 3 (in more detail, with the focus on the compression and expansion stroke) and 4 (consecutively).

Undeniably, the cylinder pressure traces exhibit a high degree of variation from cycle to cycle (excluding the first cycle, the maximum difference observed between two consecutive cycles' peak pressures was almost 38 bar). Due to the low wall temperature during cold starting, the air-charge in the cylinder could not always reach temperatures capable of fully vaporizing the injected fuel. Consequently, formation of a combustible air-fuel mixture was partially prohibited during some cycles, ultimately leading to the combustion instability demonstrated in Fig. 4. One key parameter here is the low injection pressure in the mechanical fuel pump being associated to the low cranking speed. This led to poor spray penetration, atomization and ultimately fuel evaporation. Furthermore, the synergistic effect of a) the low coolant temperature, which led to increased heat loss to the walls, b) the low lubricating oil temperature, which caused high frictional losses, and c) the low engine rotational speed that allowed more time for the above mentioned two losses to develop and also increased the blow-by losses through the piston rings, all resulted in low compression pressures (Cheng et al., 2004), eventually leading to incomplete combustion during various cycles but not starting failure.

Closer examination of the compression curves in the indicator diagrams of Fig. 3 confirms this fact. During the early starting cycles (stage 1), the compression pressure assumed significantly lower values compared with the stabilization phase and the final idling conditions. As already argued, this is attributed to the low engine speeds that allowed more time for heat and blow-by losses to develop, as well as due to the

increased rate of heat transfer to the cold cylinder walls. Both factors reduce the enthalpy of the working medium, lowering the engine ‘effective’ compression ratio and ultimately the gas pressure during compression.

Confirming the results of previous research for naturally aspirated diesel engine operation (Henein et al., 1992), an important finding from the analysis of the stage 1 cold starting pressure diagrams in Fig. 4 is that as the starting event advances, combustion development from cycle to cycle is not getting gradually more stable. Instead, it exhibits an intermittent behavior, i.e., a succession of complete and partial combustion events are encountered in a not necessarily consecutive manner. It is the specific in-cylinder conditions during one cycle that affect in a positive or negative way the next cycle, and lead to a series of firing and misfiring cycles. Previous research (Osuka et al., 1994) has indicated that during the ignition cycles, compression of residual fuel from the preceding misfiring cycle(s) causes cold flame reactions, which lead to the formation of an activated environment enabling ignition to occur; for the current investigation, this seems to be the case for cycles No. 2, 4, 6, 8, 13 and 15 in Figs 3 and 4.

The succession of firing and misfiring cycles affects the amount of produced work by the engine too, and is also reflected into the highly pulsating form of the engine acceleration in the middle-left sub-diagram of Fig. 2. With the exception of the vast acceleration rate during the first 3 cycles owing to the assistance of the electric starter, the engine accelerates or decelerates during starting in an unstable manner at least for a period of 6 seconds (30 cycles).

Warm and hot starting tests No. 2, 3 and 4

The next three tests were performed under gradually increasing coolant temperatures. They are denoted as ‘warm’ starting tests No. 2 and 3, and hot starting test No. 4 (see also Table 2), with the respective coolant temperatures being 35, 60 and 80^{o}C. Fig. 5 illustrates the development of the engine speed, peak cylinder pressure and turbocharger boost pressure and speed. Although the final idling speed of tests No. 2 and 3 is slightly higher than the one during the cold and the hot starting event, the results can still be considered comparable.

Obviously, the hotter cylinder and exhaust manifold walls during tests No. 2, 3 and 4 were the influential factors in Fig. 5 for any differences observed between them and

also between these tests and the cold starting one. The thermal status of the engine at the fully warmed-up conditions as well as the required idling speed affected the turbocharger response too (upper sub-diagrams in Fig. 5); the latter accelerated much faster compared to the cold starting test of Fig. 2, owing to the considerably higher exhaust gas energy content; the latter originated in the lower heat loss to the hotter or even fully warmed-up cylinder and exhaust manifold walls. Not surprisingly, the turbocharger accelerated faster the higher the coolant temperature of the starting test. It can be concluded that with higher coolant temperatures, turbocharger lag is becoming less critical during engine starting, reducing the discrepancy between fuelling and air-supply; it is not surprising then that the latter phenomenon is responsible for a subsequent reduction in soot emissions (Rakopoulos and Giakoumis, 2009).

The much more favorable in-cylinder conditions during the warm and hot starting tests compared to the cold starting one are also reflected into smaller-extent combustion instability phenomena, particularly throughout the early, critical engine cycles; this was also the result reached in (Armas et al., 2013). Fig. 6 lends support to this argument by depicting the indicator diagrams during the first 15 cycles of each warm and hot starting test. Moreover, a direct comparison of the cylinder pressure data between cold, warm and hot starting tests is illustrated in Fig. 7; in this figure, the maximum cylinder pressure and the difference in the peak cylinder pressures between consecutive cycles are demonstrated.

Clearly, with the increase in the coolant temperature in Fig. 6:

a) the hotter cylinder manifold walls lowered significantly the heat loss from the working medium, allowing faster fuel evaporation and consequently mixture preparation, and

b) the higher lubricant oil temperature, reduced the amount of friction losses compared to the cold starting case.

As a result, the risk of combustion failure was significantly reduced, and any combustion instability phenomena experienced were milder, although not absent; the same holds true for the absolute values of peak cylinder pressures in Figs 6 and 7, which, with the increase in the coolant temperature, were kept at lower levels too, influenced decisively by the decrease in the ignition delay period (as well as by the different response of the fuel pump rack that resulted in different fuel supply between Tests No 1 and 4 for achieving and maintaining the same idling speed). Not surprisingly,

the peak cylinder pressure graph line during the hot starting test is almost straight (continuous line in the lower sub-diagram of Fig. 7) as opposed to the ones for the tests conducted under lower coolant temperatures, where significant irregularities are observed. The latter irregularities are further, and more comprehensively, highlighted in the upper sub-diagram of Fig. 7, in the form of the difference in the peak cylinder pressure between consecutive cycles; this difference can reach up to almost 38 bar for the cold starting test compared with less than 10 bar for the hot starting one. Even higher degree of irregularity would be experienced were the ambient temperature below 0^{o}C instead of the rather moderate 20^{o}C of the cold starting experimented in the present work.

To relate the differences between the various starting tests, Table 4 quantifies the results from a statistical analysis performed on the cylinder pressure data; it provides for each tested case (and for the instrumented cylinder), the average, minimum and maximum peak pressure, the peak cylinder pressure standard deviation, as well as the number of incidents with a higher than 10, 20 or 30 bar difference between *successive* cycles. In particular the last three columns of Table 4 are indicative of the smoother development of the starting event that is experienced with the increase in the coolant temperature. Interestingly, the data for the 60^{o}C starting indicate slightly rougher operation compared to the 35^{o}C; however, these differences become milder when more engine cycles are taken into account.

It is also worth mentioning the much smaller peak cylinder pressures during the hot starting test compared to the cold (or the warm tests), indicative of the shorter and less abrupt premixed phase experienced the higher the cylinder wall temperature.

Further, Fig. 8 illustrates the engine acceleration (both in rpm/engine cycle and in rpm/s) for the two ‘extreme’ cases examined thus far, i.e., the cold and the hot starting (both conclude to almost the same idling speed). Again, the cylinder pressure irregularities depicted in Fig. 7 and quantified in Table 4 are reflected here. A direct comparison between Figs 4, 6 (for the hot starting data only) and 8 indicates that the high rate of acceleration after a firing cycle reduces the time available for the physical and chemical processes to be completed prior to TDC; this can also be documented in various occurrences for the cold starting test in Fig. 3, where it is made obvious that throughout the early starting cycles, ignition starts later in the cycle, after TDC, following the increased ignition delay period ‘imposed’ by the cold cylinder walls. Likewise, after a

misfiring cycle or partially fired cycle (characterized by incomplete combustion), engine rotational speed generally decreases allowing more time for pre-ignition chemical reactions around TDC, thus favoring ignition in the next cycles (Arcoumanis and Yao, 1994). The considerably milder form of cylinder pressure irregularities during the hot starting test are reflected into smaller acceleration discrepancies in Fig. 8 compared to the cold starting event.

In general, it is observed for the current cases (including the cold starting one) that the engine needed at least 20 cycles in order for the combustion to achieve an acceptable degree of stability, without any incident of starting failure.

Lastly, Fig. 9 compares the cylinder pressure development between the first stage of the hot starting test (cycles No. 1–15) with the 'stabilization' phase (cycles No. 55–80). Not surprisingly, combustion has become more stable later in the starting process, with lower values of maximum cylinder pressure (61.1 bar compared with 78 bar, as regards the average values) and smaller differences between consecutive cycles. However, instability phenomena are still apparent (see for example cycles No. 70, 71 and 72), a fact indicating that even after 12 seconds, complete combustion stabilization has not been achieved, even for the hot starting operation (discussed in more detail, and also quantified, later in the text in Section 4.4). The latter observation can also be attributed to the combustion cyclic variability, which, in diesel engines, is more intense at idling compared to full load operation.

Hot starting tests No. 5 and 6 with biofuel blends

The final two tests were actually a reproduction of the hot starting test No. 4, this time conducted with the engine running on different biofuel blends; it is tests No. 5 and 6 (in Table 2) that are under investigation and discussion in this section. It is reminded that for test No. 5, the blend used consisted of 70% diesel fuel and 30% bio-diesel (v/v), while for test No. 6 it was 75% diesel fuel and 25% *n*-butanol (v/v). The behavior of the engine for each one of these three tests, as exhibited in the next three figures (10, 11 and 12), arises, at least in part, owing to the different injection and combustion process of each biofuel blend. It is worth pointing out that, as is the case in all similar investigations, the fuel system of the engine is optimized for neat diesel fuel operation, and there was no change or different calibration applied with the use of biofuels. The

differing physical and chemical properties of each constituent of the blends resulted, however, in alteration of the fuel delivery, dynamic injection timing, fuel spray dispersion, wall impingement rate, ignition delay, as well as fuel evaporation and mixing rates. As a result, the premixed and diffusion parts of combustion varied between the three blends; in particular, the presence of oxygen in the biofuel blends altered the local fuel-air equivalence ratios, favoring or preventing the initiation of combustion, and, in combination with the different cetane number, shifted a greater part of combustion to the premixed (particularly for alcohol-diesel blends) or diffusion phase.

Figure 10 demonstrates the main engine and turbocharger parameters' development during the hot starting with the emphasis placed again on the evolution of the peak cylinder pressure for all three fuel blends. It seems that the biofuel blend type does not affect significantly the engine and turbocharger hot starting response and performance, at least for blends up to 30% by vol. of bio-diesel or *n*-butanol as the ones tested here. Closer inspection of the engine speed evolution in Fig. 10, however, reveals that the n-butanol blend accelerates slightly slower compared to the other two blends, a fact that also influences the results depicted later in Fig. 13. As with all the test cases discussed previously, independently of the fuel blend used, the initial sharp increase in the engine speed was due to the electric starter action.

A further notable finding concerns the development of combustion, which is supported by Fig. 11 depicting the respective cylinder pressure diagrams during the first 25 cycles of the hot starting event for each fuel blend. It is revealed from this figure that a higher degree of combustion instability is experienced by the biodiesel blend, whereas its *n*-butanol counterpart behaves in a slightly more stable manner (the neat diesel fuel too) despite the lower alcohol cetane number. This is also documented in the lower sub-diagram of Fig. 12. In the same figure, it is also shown that throughout the biodiesel blend hot starting, the engine experienced higher cycle-by-cycle peak cylinder pressure variability; the latter is further quantified in Table 5. Clearly, the high value of the peak cylinder pressure deviation for the biodiesel blend in Table 5 indicates more intense combustion instability, probably originating in the methyl ester's high viscosity and initial boiling point (both higher than the respective values of the other two tested blends in Table 3). On the other hand, a major reason for the higher absolute values of gas pressures experienced for the *n*-butanol blend is, most likely, its lower cetane number, which leads to longer ignition delay, hence more abrupt premixed combustion.

Interestingly, misfire was not an issue for either biofuel blend tested (even for the lower-cetane-number diesel/*n*-butanol one), most probably owing to the already fully-warmed-up engine conditions.

Overall, it seems that addition of biofuel in the fuel renders hot starting less stable with higher pressure irregularities. Armas et al. (2015) for *n*-butanol/diesel blends and Broach et al. (2014) for biodiesel ones reported similar findings, nonetheless during the much more demanding operation of cold starting. Notice in Table 5 the difference between the maximum and the minimum recorded cylinder pressure, which is 40 bar for the biodiesel blend and almost 30 bar for the *n*-butanol one compared with 'only' 24 bar for the neat diesel operation.

It is not surprising then, that the higher cylinder pressure irregularities of the two biofuel blends are also reflected into more unstable engine acceleration, demonstrated in Fig. 13, compared to the neat diesel operation. As was the case in Fig. 8, the abrupt deceleration for all blends after the 3rd cycle (approx. 1.5 s) is due to the disengagement of the electric starter.

It is reminded here, that the engine acceleration depicted in Fig. 13 is the result of various torque terms acting on the engine crankshaft as described by the following equation (application of Newton's 2nd law of motion for rotating systems)

$$M_e(\varphi) - M_L(\varphi) = \Theta \frac{d\omega}{dt} \qquad (1)$$

with $M_e(\varphi)$ the instantaneous engine torque (comprising gas, inertia and friction forces), $M_L(\varphi)$ the load torque ($\propto \omega^2$ for the hydraulic brake employed here, which is of considerable moment of inertia, and due to its construction of not necessarily 'linear' response when abrupt transients are demanded), and Θ the total (engine+brake) moment of inertia, including also shaft stiffness and damping effects. From the above terms, the engine inertia and the load torque are related to the engine speed only, whereas the friction term incorporates both gas and engine speed terms, with its behavior during starting being of highly unstable and non-linear nature.

Overall data during the stabilization phase

Figs 14 and 15 demonstrate and Table 6 summarizes some interesting data for all the conducted starting tests regarding the difference between the initial starting phase (cycles 2-10, denoted as the first engine cycle decade, incorporating also the 3 cranking cycles) and the 10th decade (cycles 91-100), almost 15 s into the engine operation.

For all the examined starting tests, irrespective of coolant temperature or fuel blend, the peak cylinder pressure exhibits a continuous, uninterruptible decreasing trend during the stabilization phase, as is evidenced in Fig. 14 and documented in the first two rows of Table 6; the difference in the average cylinder pressures between the 1st and 10th decade is at least 10 bar for all cases. Even higher differences are observed when the maximum (for each cycle decade) cylinder pressures are considered (3rd and 4th row in Table 6), reaching now up to 28 bar for the cold starting test and 20 bar for most of the other tests.

The most interesting feature of the starting process, however, is documented in the last two rows of Table 6, which focus on the peak cylinder pressure standard deviation for the 1st and the 10th engine cycle decade. For all hot starting tests, a considerable degree of peak cylinder pressure deviation is apparent even 15 s after starting of the engine, in particular for the neat diesel and the diesel/biodiesel blend. It is worthwhile mentioning that the peak cylinder pressure standard deviation for the diesel and the diesel/biodiesel blends' hot starting is higher between cycles 91-100 rather than during cycles 2-10. Fig. 15 expands the data of Table 6 by showing the respective standard deviation for all ten cycle decades (up to cycle No. 100), where it is again made obvious, that the lower the coolant temperature the lower the standard deviation gets during the warm-up phase. Nonetheless, a considerable degree of deviation is still experienced even after 100 cycles or almost 15 s, which does not seem to become smoother even for the hot starting operation (Pham et al., 2014).

Summary and Conclusions

A fully instrumented test bed installation was developed in order to study the combustion instability of a medium-duty, turbocharged diesel engine during various starting tests conducted at different coolant temperatures (ranging from 20 to 80^{o}C) and fuel blends (neat diesel oil, blend of diesel with 30% biodiesel, and blend of diesel with 25% *n*-

butanol v/v). The basic conclusions derived from the current investigation and for the specific engine-brake configuration can be summarized as follows:

- Combustion instability was significant, particularly during cold starting. Repeatedly high differences were encountered as regards the peak cylinder pressure between successive cycles, reaching up to almost 38 bar. Actually, the cold starting event was characterized by a series of engine cycles with complete and incomplete combustion for several seconds after initiation of the starter.
- The initial low cylinder wall temperature throughout cold starting prohibited fast and full mixture preparation (mainly fuel vaporization) and led to abrupt heat release after the prolonged ignition delay, resulting in steep cylinder pressure rise and high peak pressures.
- The thermal status of the engine played a key role with respect to combustion stability and turbocharger response. As the engine was operated at hotter coolant temperatures, combustion became more stable with lower values in both peak cylinder pressure and difference between consecutive cycles' cylinder pressures; at the same time, the turbocharger accelerated faster producing higher boost pressure.
- Combustion behavior and stability during the first hot starting cycles were affected more by the biodiesel blend and somewhat less by the *n*-butanol one; the latter exhibited also higher absolute gas pressure values. The evolution of the whole (hot) starting event as regards engine and turbocharger speed response did not differ substantially between the biofuel blends, probably owing to the already fully warmed-up conditions of the test.
- For all the examined blends, even several seconds after the starting test, combustion had not stabilized completely, with instability phenomena still apparent, although of predictably lower magnitude. Such instability phenomena characterise diesel engine operation at idle, usually referred to as cyclic variability.

Nomenclature

CA crank angle

CI	compression ignition
CO	carbon monoxide
DPF	diesel particulate filter
HC	hydrocarbons
ME	methyl ester
NEDC	new European driving cycle
NO_x	nitrogen oxides
PM	particulate matter
SI	spark ignition
TDC	top dead center
v/v	by volume
WLTP	Worldwide harmonised Light vehicle Test Procedure

565 # References
566

567 Arcoumanis, C. and Yao, X.G. (1994). “Transient smoke and unburnt hydrocarbon emissions
568 during cold-start in a turbo-charged DI diesel engine”. *Institution of Mechanical Engineers*,
569 Seminar on ‘Transient performance of engines’, pp.43–60.
570 Cardenas, M., Gomez, A., Armas, O. (2015). “Pollutant emissions from starting a common rail
571 diesel engine fuelled with different biodiesel fuels”. *J. Energy Eng*., 142, Article No.
572 4015012.
573 Armas, O., Gomez, A., Ramos, A. (2013). “Comparative study of pollutant emissions from
574 engine starting with animal fat biodiesel and GTL fuels”. *Fuel,* 113, 560−570.
575 Armas, O., Garcia-Contreras, R., Ramos, A., Lopez, A. (2015). "Impact of animal fat biodiesel,
576 GTL and HVO fuels on combustion performance and pollutant emissions of a light-duty
577 diesel vehicle studied under the NEDC". *J. Energy Eng*., 141, Article No. 4014009.
578 Bielaczyc, P., Merkisz, J., Pielecha, J. (2001). “Investigation of exhaust emissions from DI diesel
579 engine during cold and warm start”; SAE Paper No. 2001-01-1260.
580 Broatch, A., Tormos, B., Olmeda, P., Novella, R. (2014). “Impact of biodiesel fuel on cold starting
581 of automotive direct injection diesel engines”. *Energy*, 73, 653−660.
582 Cheng, K.Y., Shayler, P.J., Murphy, M. (2004). “The influence of blow-by on indicated work
583 output from a diesel engine under cold start conditions”. *Proc. Inst. Mech. Eng., Part D, J.*
584 *Automobile Eng.*, 218, 333–340.
585 Giakoumis, E.G. (2012). “A statistical investigation of biodiesel effects on regulated exhaust
586 emissions during transient cycles”. *Appl. Energy*, 98, 273−291.
587 Giakoumis, E.G. (2013). “A statistical investigation of biodiesel physical and chemical properties,
588 and their correlation with the degree of unsaturation”. *Renewable Sustainable Energy*
589 *Rev.*, 50, 858−78.
590 Giakoumis, E.G., Alysandratou A. (2015). “Performance and emissions of a heavy-duty truck
591 during the UDDS driving cycle – Simulation analysis. ASCE J Energy Eng, 142, Article No.
592 E4015011.
593 Giakoumis, E.G., Rakopoulos, C.D., Rakopoulos, D.C. (2014). “An assessment of NOx
594 emissions during transient diesel engine operation with biodiesel blends”, *J. Energy Eng.*,
595 140, Article No. 4014004.
596 Giakoumis, E.G., Rakopoulos, C.D., Dimaratos, A.M., Rakopoulos, D.C. (2012). “Exhaust
597 emissions of diesel engines operating under transient conditions with biodiesel blends”.
598 *Progr. Energy Combust. Sci.*, 38, 691−715.

599 Giakoumis, E.G., Rakopoulos, C.D., Dimaratos, A.M., Rakopoulos, D.C. (2013). “Exhaust
600 emissions with ethanol or n-butanol diesel fuel blends during transient operation: a review”.
601 *Renewable Sustainable Energy Rev.*, 17, 170−90.
602 Graboski, M.S., McCormick, R.L (1998) ‘Combustion of fat and vegetable oil derived fuels in
603 diesel engines’, *Progress in Energy and Combustion Science*, Vol. 24, pp.125−64.
604 Hansen, A.C., Zhang, Q., Lyne, P.W.L. (2005). “Ethanol/diesel fuel blends - a review”. *Biores.*
605 *Technol*, 96, 277−285.
606 Henein, N.A., Zahdeh, A.R., Yassine, M.K., Bryzik, W. (1992). “Diesel engine cold starting:
607 combustion instability”. SAE Paper No. 920005.
608 Jin, C., Yao, M., Liu, H., Lee, C.F., Ji, J. (2011). “Progress in the production and application of n-
609 butanol as a biofuel”. *Renewable Sustainable Energy Rev.*, 15, 4080−4106.
610 Kobayashi, A., Kurashima, A., Endo, S. (1984). “Analysis of cold start combustion in a direct
611 injection diesel engine”. SAE Paper No. 840106.
612 Lapuerta, M., Armas, O., Rodriguez-Fernandez, J. (2008). “Effect of biodiesel fuels on diesel
613 engine emissions”. *Progr. Energy Combust. Sci.*, 34, 198−223.
614 Mathis, U., Mohr, M., Forss, A.M. (2005). “Comprehensive particle characterization of modern
615 gasoline and diesel passenger cars at low ambient temperatures”. *Atmos. Environ.,* 39,
616 107−117.
617 Osuka, I., Nishimura, M., Tanaka, Y., Miyaki, M. (1994). “Benefits of new fuel injection
618 technology on cold startability of diesel engines – improvement of cold startability and
619 white smoke reduction by means of multi injection with common rail fuel system (ECD-
620 U2)”. SAE paper No. 940586.
621 Pham, P.X., Bodisco, T.A., Ristovski, Z.D., Brown, R.J., Masri, A.R. (2014). “The influence of
622 fatty acid methyl ester profiles on inter-cycle variability in a heavy duty compression
623 ignition engine”. *Fuel*, 116, 40–150.
624 Phatak, R., Nakamura, T. (1983). “Cold startability of open chamber direct injection diesel
625 engines. Part I: measurement technique and effects of compression ratio”. SAE Paper No.
626 831335.
627 Rakopoulos, D.C. (2015). "Comparison of combustion, performance and emissions of an HSDI
628 engine operating on blends of diesel fuel with ethanol, n-butanol, or butanol isomer ether
629 DEE", *J. Energy Eng*., 141, Article No. C4014001.
630 Rakopoulos, C.D., Giakoumis, E.G. (2009). *Diesel engine transient operation – principles of*
631 *operation and simulation analysis,* Springer, London.
632 Rakopoulos, C.D., Dimaratos, A.M., Giakoumis, E.G., Rakopoulos, D.C. (2011a). “Study of
633 turbocharged diesel engine operation, pollutant emissions and combustion noise radiation

during starting with bio-diesel or n-butanol diesel fuel blends". *Appl. Energy*, 88, 3905−3916.

Rakopoulos, C.D., Dimaratos, A.M., Giakoumis, E.G., Rakopoulos, D.C. (2011b). "Investigating the emissions during acceleration of a turbocharged diesel engine operating with bio-diesel or n-butanol diesel fuel blends". *Energy*, 35, 5173−5184.

Randazzo, M.L., Sodre, J.R. (2011). "Cold start and fuel consumption of a vehicle fuelled with blends of diesel oil – soybean biodiesel – ethanol". *Fuel,* 90, 3291−3294.

Watson, N., Janota, M.S. (1986). *Turbocharging the internal combustion engine*, McGraw-Hill, London.

Yao, M., Wang, H., Zheng, Z., Yue, Y. 2010). "Experimental study of n-butanol additive and multi-injection on HD diesel engine performance and emissions", *Fuel*, 89, 2191−2201.

Table 1 - Engine and turbocharger specifications

Engine model and type	Mercedes-Benz OM 366 LA, 6 cylinder, in-line, 4-stroke, compression ignition, direct injection, water-cooled, turbocharged, after-cooled, with bowl-in-piston
Speed range	800–2600 rpm
Maximum power	177 kW @ 2600 rpm
Maximum torque	840 Nm @ 1250–1500 rpm
Engine total displacement	5,958 cm^3
Bore/Stroke	97.5 mm/133 mm
Compression ratio	18:1
Fuel pump	Bosch PE-S series, in-line, 6-cylinder with fuel limiter
Static injection timing	5±1° crank angle before TDC (at full load)
Turbocharger model	Garrett TBP 418-1 with internal waste-gate
After-cooler	Air-to-Air

Table 2 - List and basic data of the conducted starting tests

Test No.	**Transient Schedule**	**Idling Speed (rpm)**	**Coolant Temperature (ºC)**	**Fuel Blend**
1.	Cold starting	900	20	Neat diesel
2.	'Warm' starting	1010	35	Neat diesel
3.	'Warm' starting	1010	60	Neat diesel
4.	Hot starting	950	80	Neat diesel
5.	Hot starting	950	80	70% diesel – 30% biodiesel
6.	Hot starting	950	80	75% diesel – 25% n-butanol

Table 3 – Properties of the diesel fuel and the biofuels used in the analysis

Fuel property	diesel fuel	sunflower ME	cottonseed ME	*n*-butanol
Density at 20ºC, kg/m^3	837	880	885	810
Cetane number	50	50	52	~25
Lower calorific value, MJ/kg	43	37.5	37.5	33.1
Kinematic viscosity at 40ºC, mm^2/s	2.6	4.4	4	3.6$^+$
Boiling point ºC	280	345	345	118
Latent heat of evaporation, kJ/kg	250	230	230	585
Oxygen, % weight	0	10.9	10.9	21.6
Stoichiometric air-fuel ratio	15.0	12.5	12.5	11.2
Molecular weight, kJ/kmol	170	284	284	74

$^+$Measured at 20ºC

Table 4 – Statistical analysis of the peak pressures recorded for each starting test with neat diesel oil, during the first 15 engine cycles

Test	Idling Speed / Coolant Temperature	Max. peak cylinder pressure	Min. peak cylinder pressure	Difference between max. and min. recorded peak cylinder pressures	Average peak cylinder pressure	Peak cylinder pressure standard deviation	Maximum difference between two successive cycles' peak pressures	No of incidents with > 30 bar difference between two successive cycles' peak pressures	No of incidents with > 20 bar difference between two successive cycles' peak pressures	No of incidents with > 10 bar difference between two successive cycles' peak pressures
1.('cold')	900 rpm / 20ºC	103.64	56.18	47.46	85.48	13.39	37.40	3	6	11
2.('warm')	1010 rpm / 35ºC	98.28	61.17	37.11	83.29	10.23	26.95	0	2	6
3.('warm')	1010 rpm / 60ºC	98.58	67.13	31.45	81.83	11.68	30.17	1	6	7
4.('hot')	950 rpm/ 80ºC	85.04	70.98	14.06	78.07	3.84	9.28	0	0	0

all pressures in bar; data excluding first cycle

678 **Table 5 –** Statistical analysis of the peak pressures recorded for each hot starting test
679 during the first 25 engine cycles with various (bio)fuel blends

Test	Fuel Blend	Maximum peak cylinder pressure	Minimum peak cylinder pressure	Difference between max. and min. recorded peak cylinder pressures	Average peak cylinder pressure	Peak cylinder pressure standard deviation	Maximum difference between two successive cycles' peak pressures	No of incidents with > 30 bar difference between two successive cycles' peak pressures	No of incidents with > 20 bar difference between two successive cycles' peak pressures	No of incidents with > 10 bar difference between two successive cycles' peak pressures
4.('hot')	D	85.65	61.72	23.93	75.28	6.74	19.31	0	0	4
5.('hot')	70% D–30% Bd	98.78	58.78	40.00	74.68	9.37	40.00	2	4	10
6.('hot')	75% D–25% But	92.33	62.95	29.38	81.54	8.30	26.56	0	2	9

680 all pressures in bar; data excluding first cycle
681 D: diesel; Bd: biodiesel; But: *n*-butanol
682
683
684
685
686 **Table 6 –** Comparison in the average and maximum peak cylinder pressure (bar) and
687 the respective standard deviation between the 1st and the 10th engine cycle decade for
688 each starting test

	Cycles	Cold starting (diesel, 20°C)	Warm starting (diesel, 35°C)	Warm starting (diesel, 60°C)	Hot starting (diesel, 80°C)	Hot starting (70% diesel / 30% biodiesel, 80°C)	Hot starting (75% diesel / 25% *n*-butanol, 80°C)
Average peak cylinder pressure	2–10	84.62	80.80	77.09	72.59	73.96	80.26
	91–100	72.83	70.94	67.48	59.89	64.04	66.82
Maximum peak cylinder pressure	2–10	103.64	93.68	98.17	85.04	86.94	90.76
	91–100	75.22	74.26	71.24	67.30	73.31	70.18
Peak cylinder pressure standard deviation	2–10	10.76	4.76	12.14	4.12	4.87	4.23
	91–100	1.62	1.66	2.56	5.15	5.38	2.40

689
690
691
692

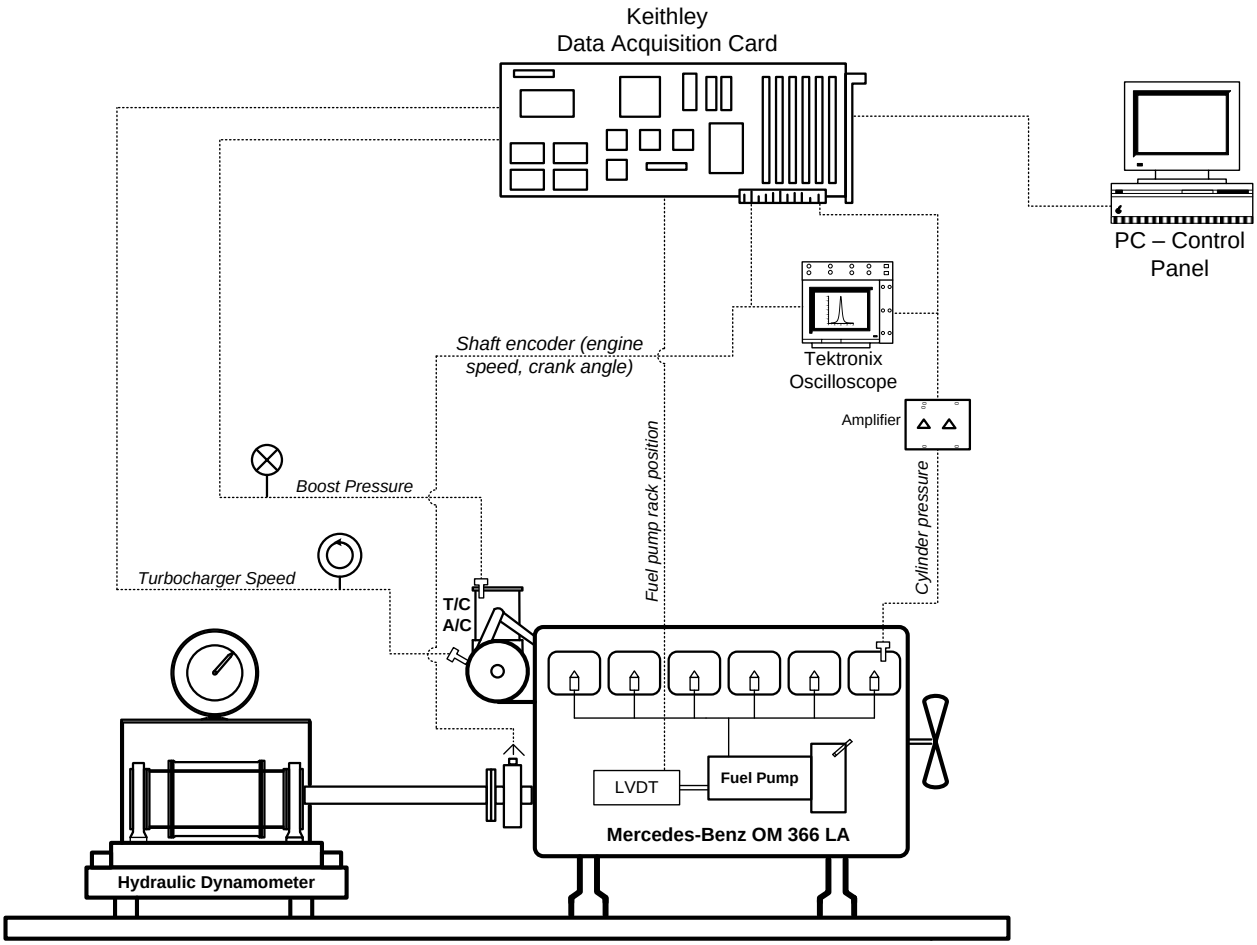

Figure 1 – Schematic presentation of the test bed installation

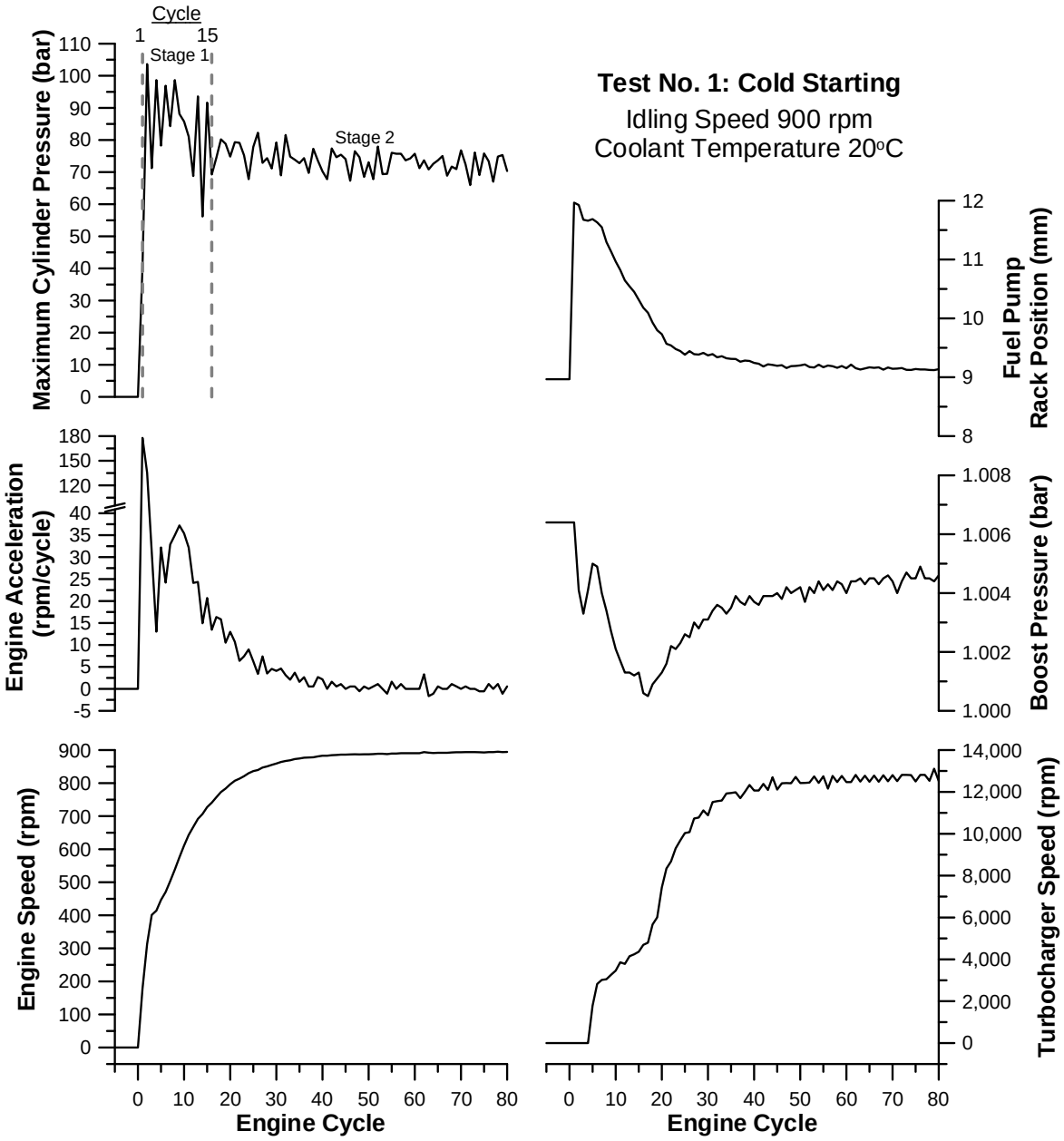

699
700
701 **Figure 2 –** Development of engine and turbocharger properties during cold starting (test
702 No. 1)
703
704

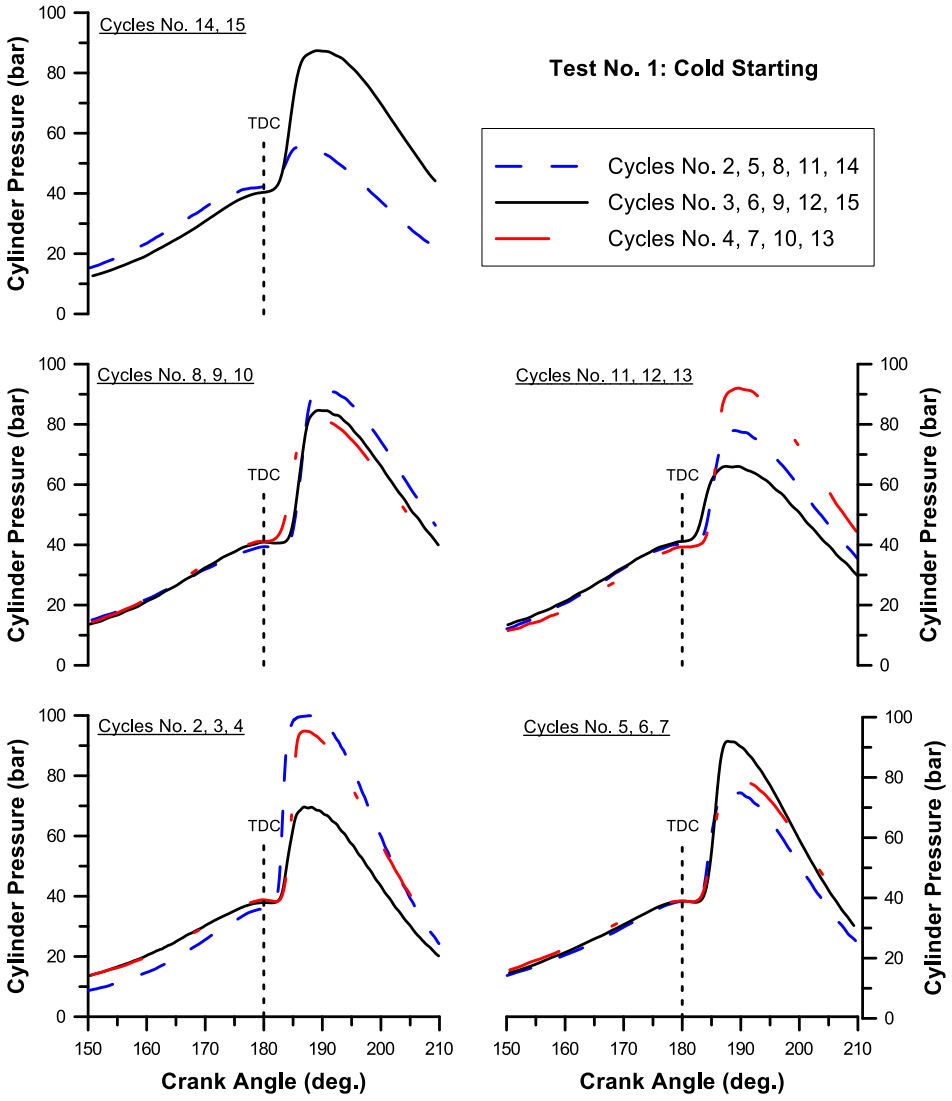

Figure 3 – Cylinder pressure diagrams from the first stage of the cold starting test No. 1

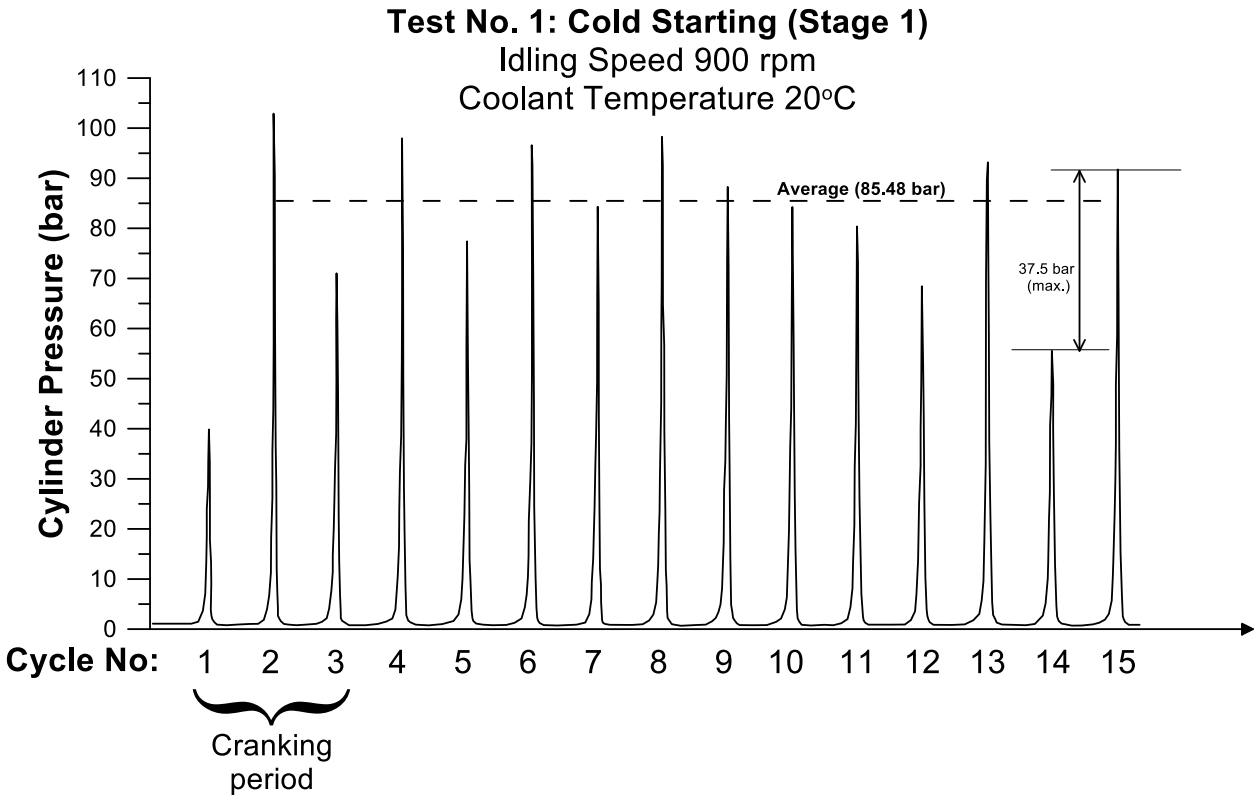

Figure 4 – Combustion instability during the first stage (15 engine cycles) of the cold starting test No. 1 (based on the indicator diagrams of Fig. 3)

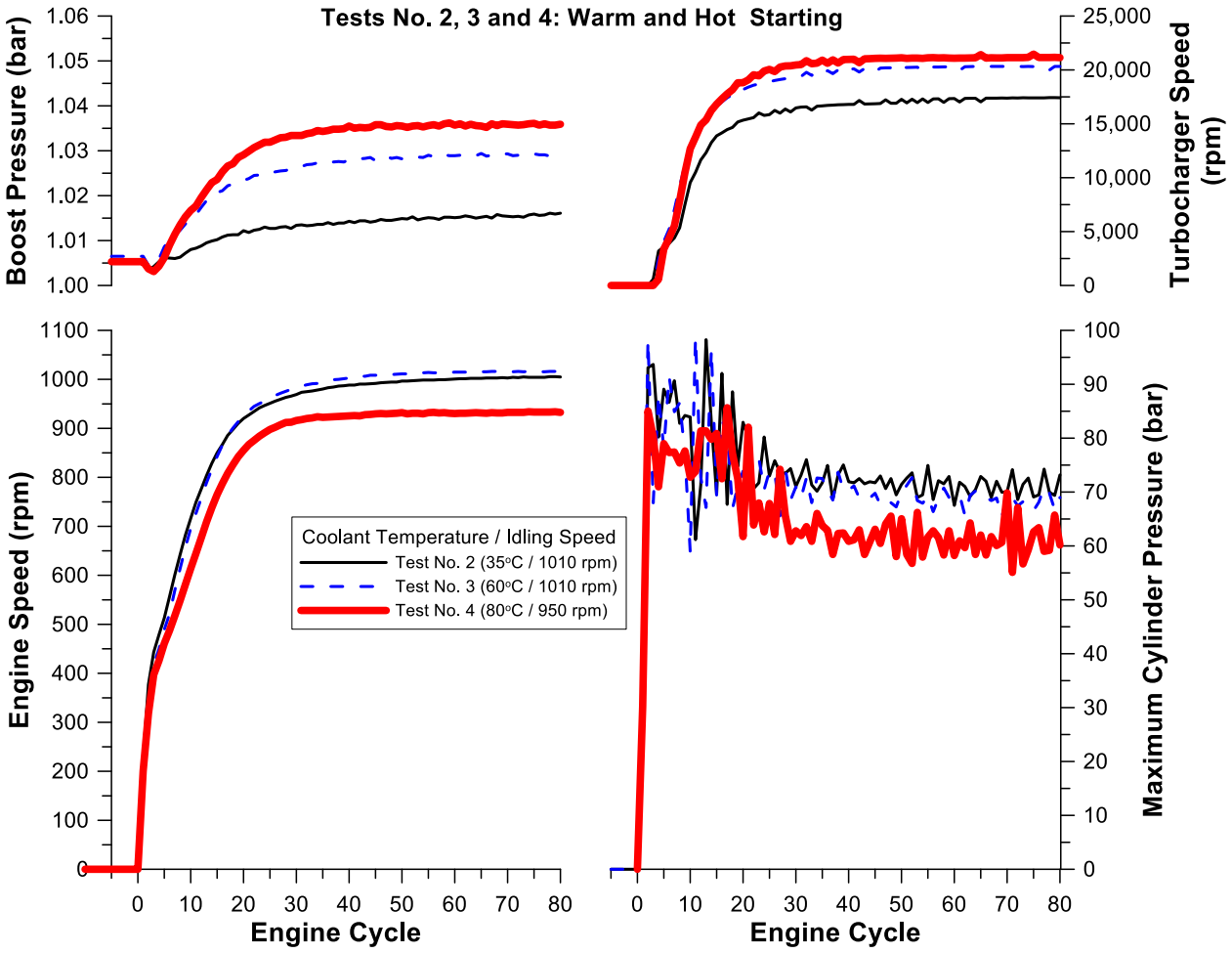

Figure 5 – Development of engine and turbocharger properties during the warm starting tests No. 2 and 3 and the hot starting test No. 4

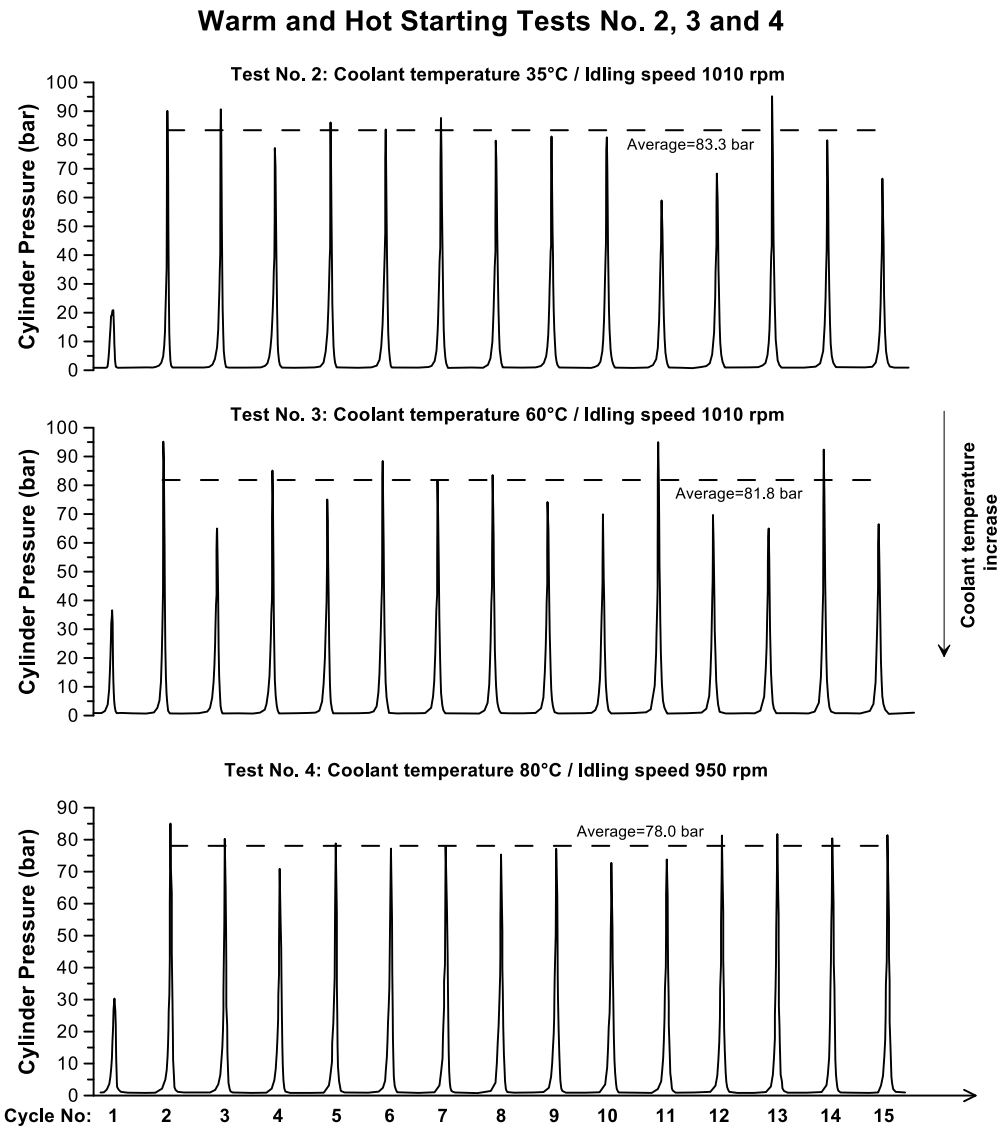

Figure 6 – Combustion instability during the warm and hot starting tests No. 2, 3 and 4 of Fig. 5

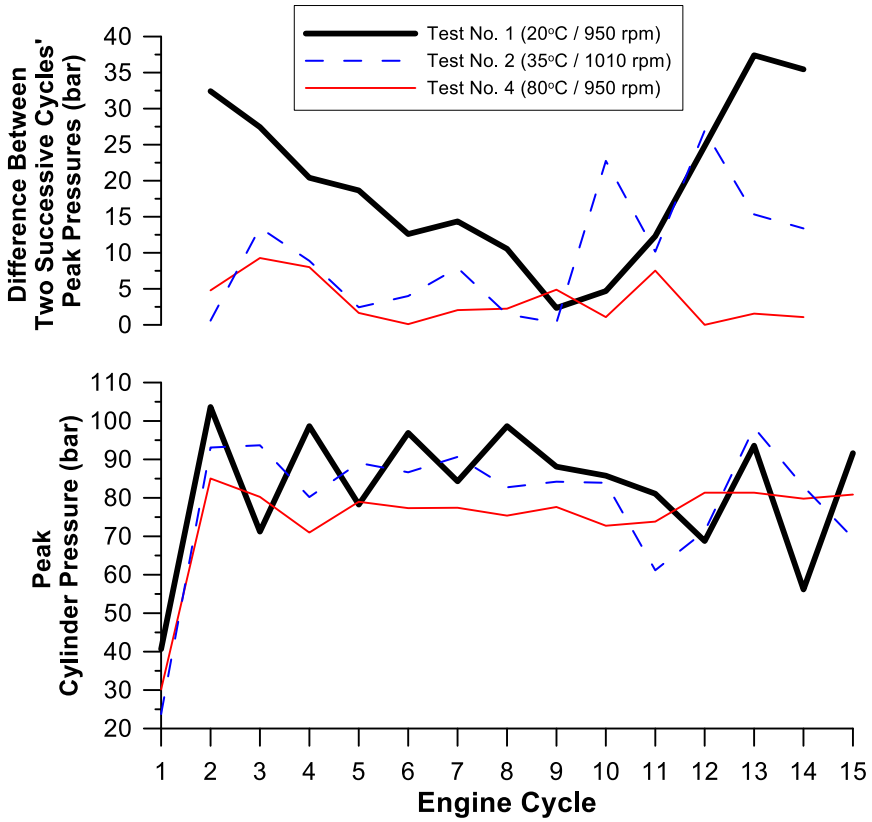

Figure 7 – Comparison of cylinder pressure data between the cold starting test No. 1, the warm starting No. 2 and the hot starting test No. 4 (neat diesel operation)

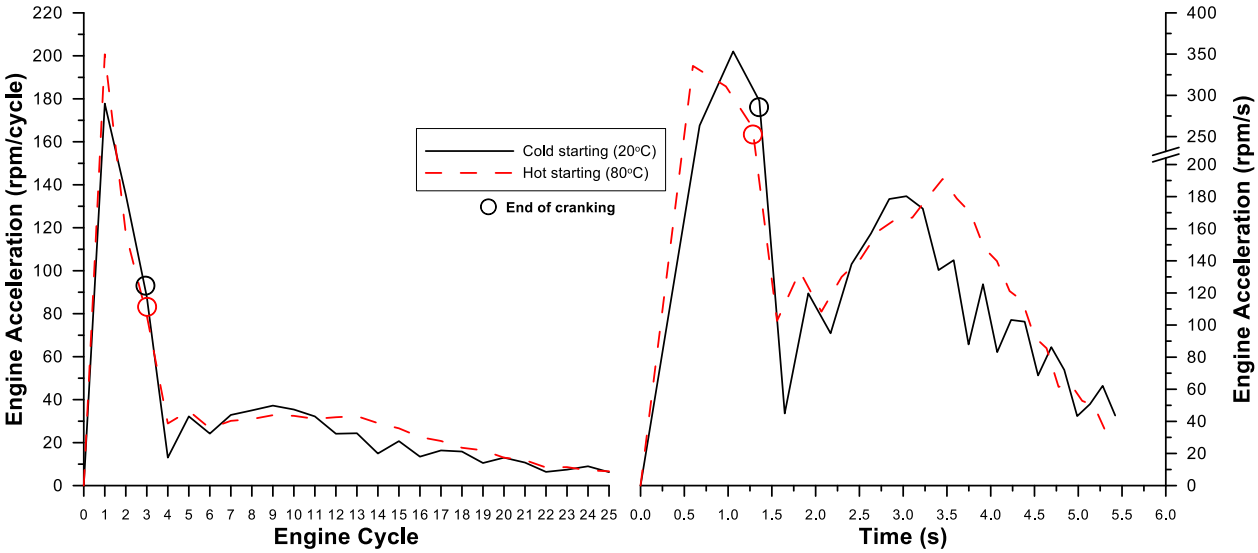

744

745 **Figure 8 –** Comparison in the engine acceleration between the cold and the hot starting

746 tests (neat diesel operation)

747

748

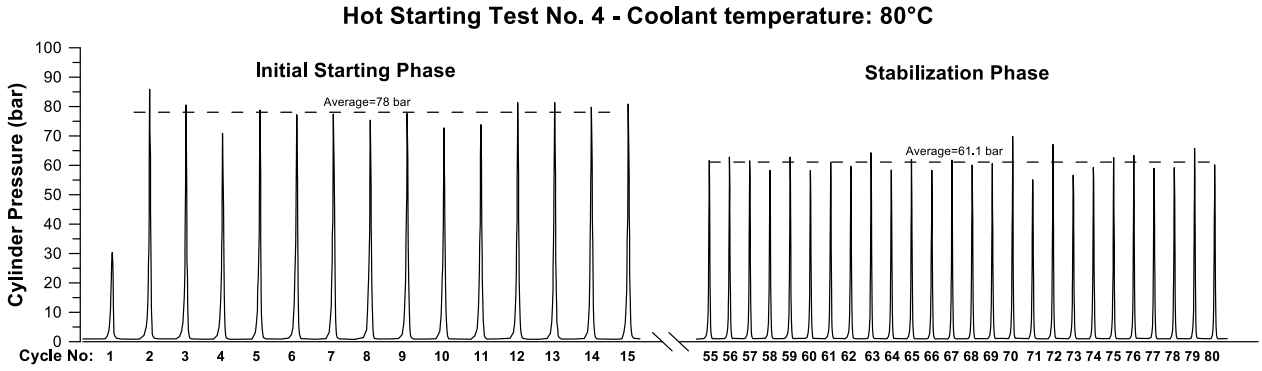

Figure 9 – Combustion instability during the initial phase (Cycles No. 1−15) and the ‘stabilization’ phase (Cycles No. 55−80) of the hot starting test No. 4 of Figure 5

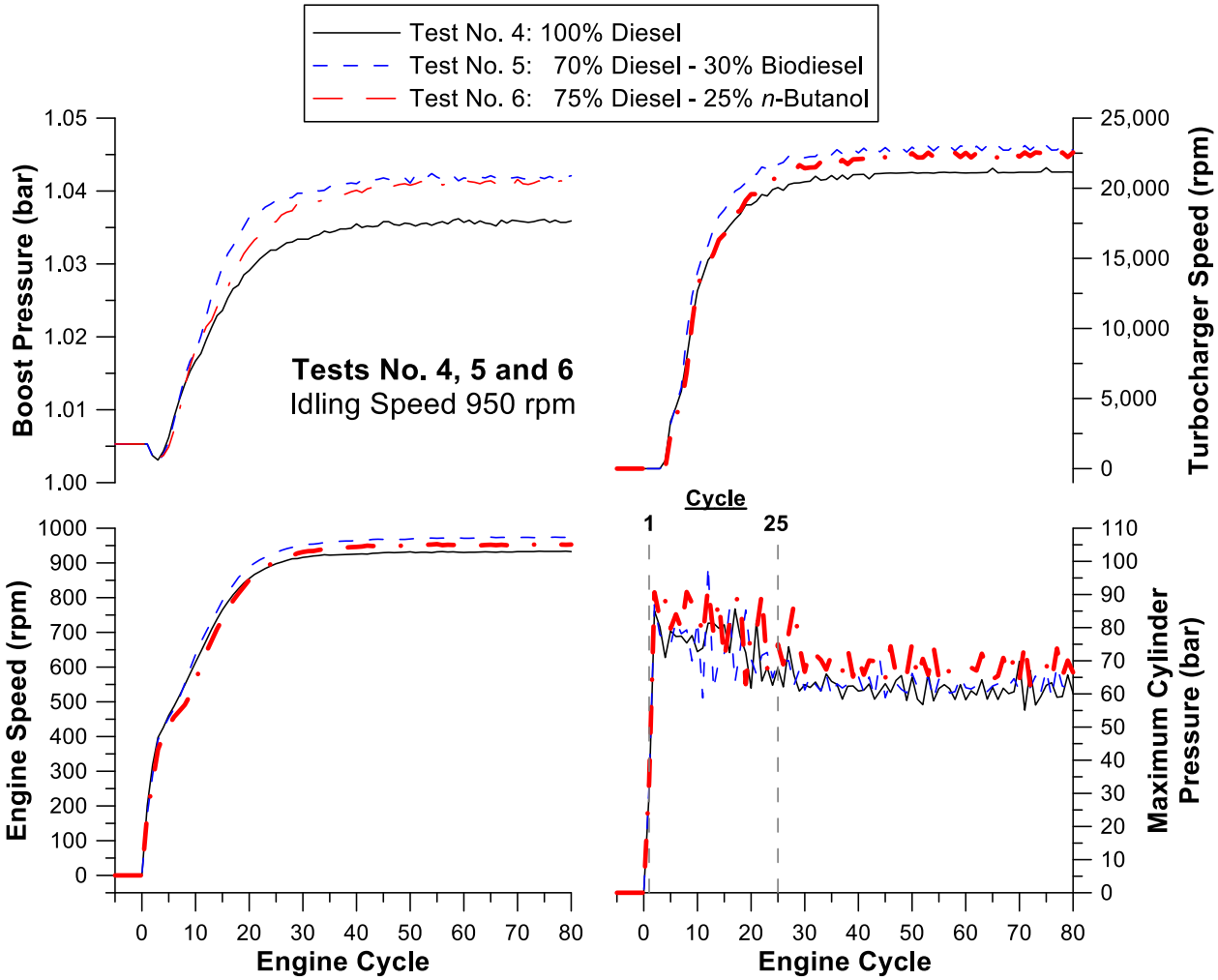

Figure 10 – Development of engine and turbocharger response during hot starting, with different fuel blends (tests No. 4, 5 and 6)

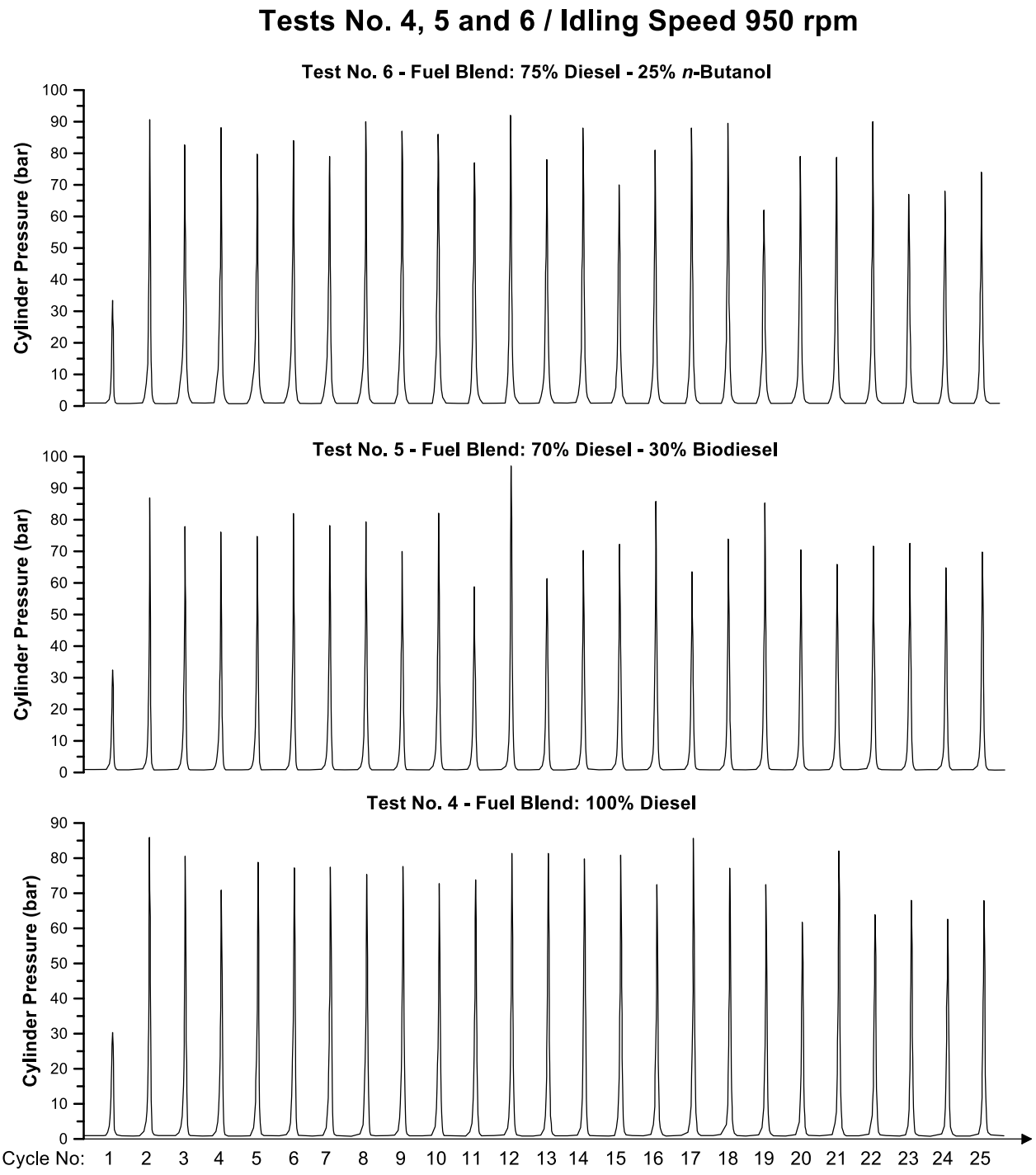

Figure 11 – Combustion instability during the first 25 cycles of hot starting with different fuel blends (tests No. 4, 5 and 6)

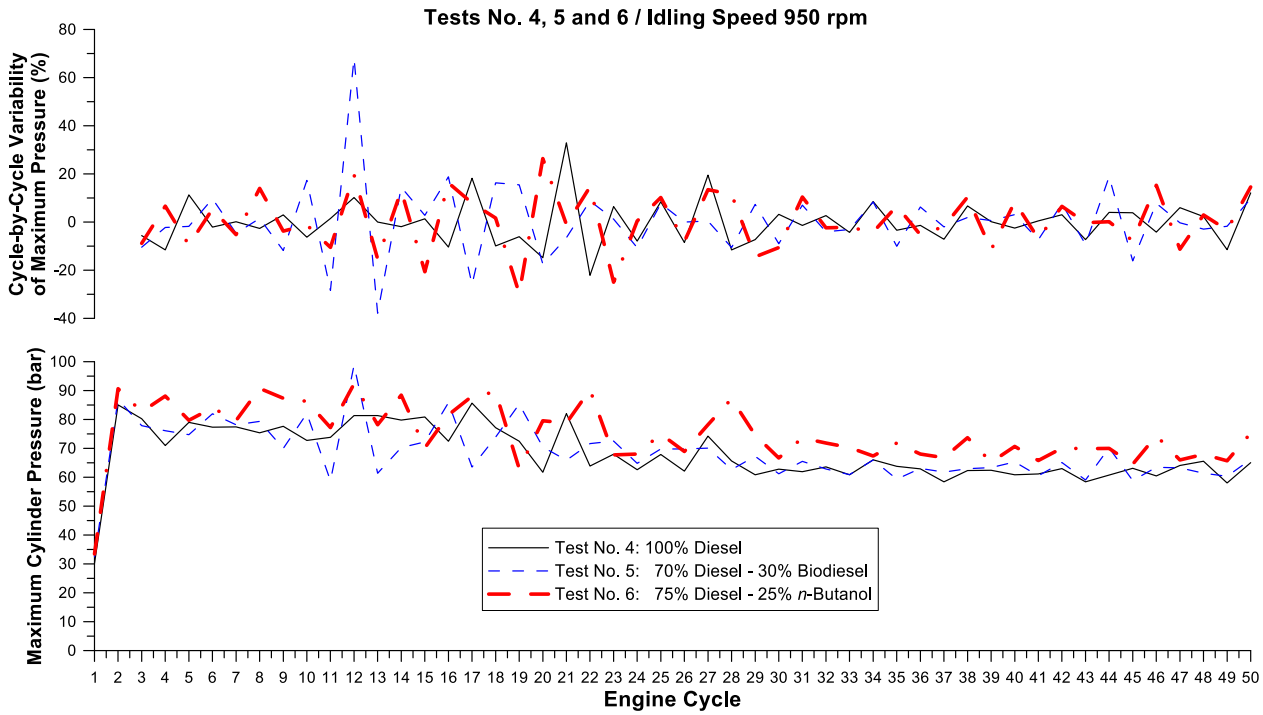

Figure 12 – Maximum cylinder pressure and its cycle-by-cycle variability during the first 50 cycles of hot starting, with different fuel blends (tests No. 4, 5 and 6)

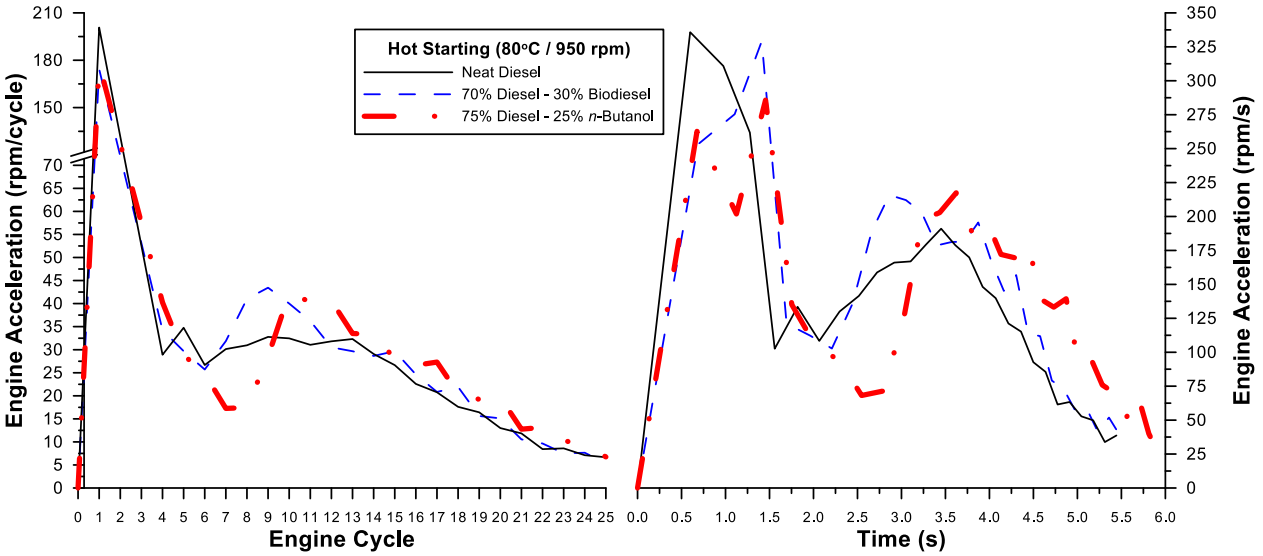

Figure 13 – Comparison in the engine acceleration during the hot starting test between the three (bio)fuel blends tested

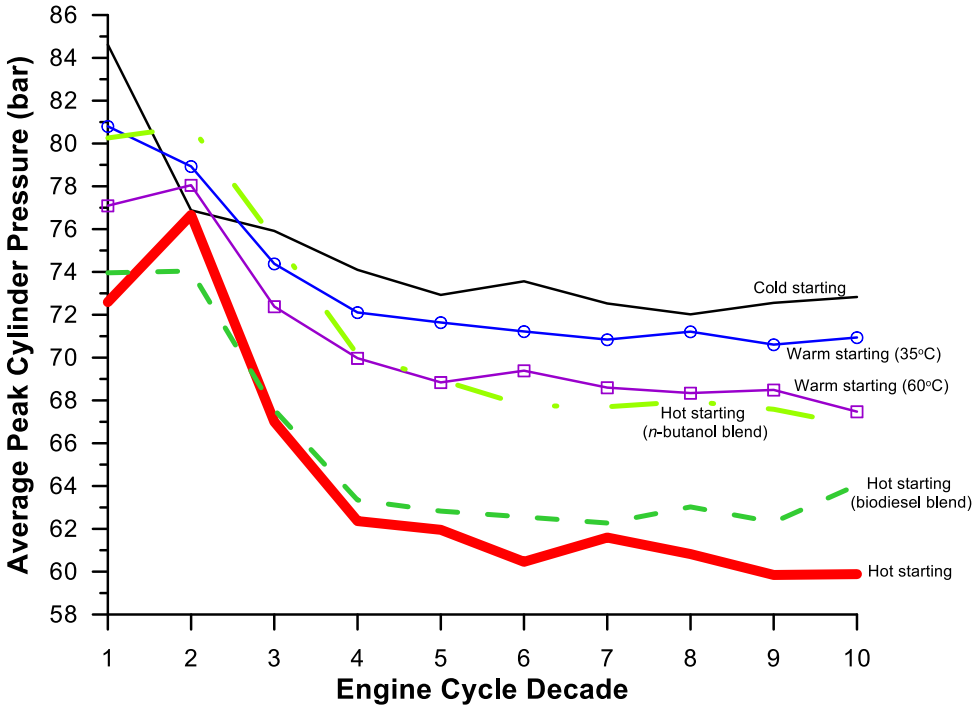

780

781 **Figure 14 –** Development in the average peak cylinder pressure during the first 10

782 engine cycle decades (cycles 2-100) for all starting tests

783

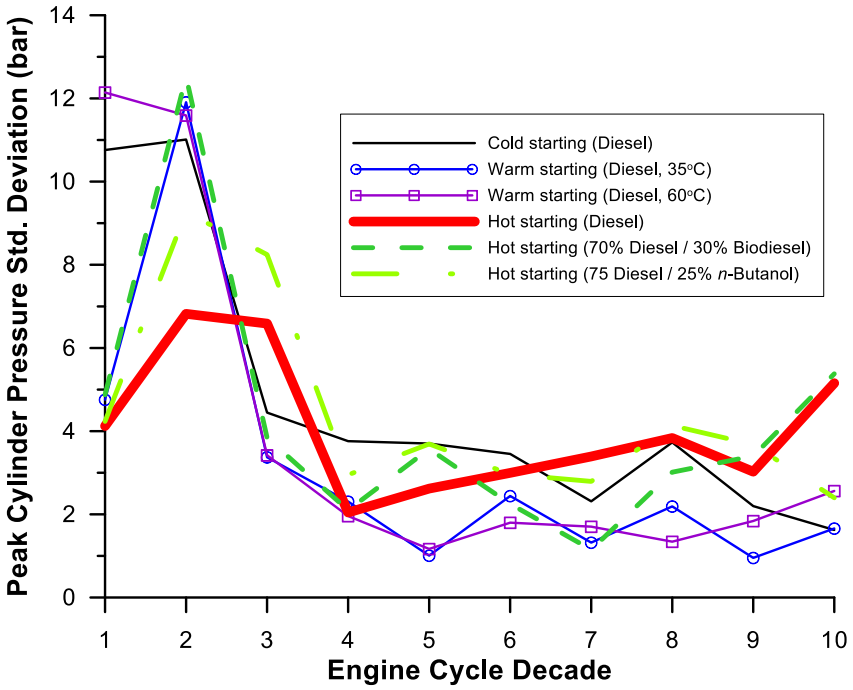

784

785 **Figure 15 –** Development in the peak cylinder pressure standard deviation during the

786 first 10 engine cycle decades (cycles 2-100) for all starting tests

787